Published in final edited form as:
J Membr Biol. 2012 July ; 245(7): 411–422. doi:10.1007/s00232-012-9465-z.

Cx43 Associates with $Na_v1.5$ in the Cardiomyocyte Perinexus

J. Matthew Rhett, **Emily L. Ongstad**, **Jane Jourdan**, and **Robert G. Gourdie**
Department of Regenerative Medicine, Medical University of South Carolina, 173 Ashley Ave, CRI Room 616, Charleston, SC 29425, USA

Abstract

Gap junctions (GJs) are aggregates of channels that provide for direct cytoplasmic connection between cells. Importantly, this connection is thought responsible for cell-to-cell transfer of the cardiac action potential. The GJ channels of ventricular myocytes are composed of connexin43 (Cx43). Interaction of Cx43 with zonula occludens-1 (ZO-1) is localized not only at the GJ plaque, but also to the region surrounding the GJ, the perinexus. Cx43 in the perinexus is not detectable by immunofluorescence, yet localization of Cx43/ZO-1 interaction to this region indicated the presence of Cx43. Therefore, we hypothesized that Cx43 occurs in the perinexus at a lower concentration per unit membrane than in the GJ itself, making it difficult to visualize. To overcome this, the Duolink protein–protein interaction assay was used to detect Cx43. Duolink labeling of cardiomyocytes localized Cx43 to the perinexus. Quantification demonstrated that signal in the perinexus was lower than in the GJ but significantly higher than in nonjunctional regions. Additionally, Duolink of Triton X-100-extracted cultures suggested that perinexal Cx43 is nonjunctional. Importantly, the voltage gated sodium channel $Na_v1.5$, which is responsible for initiation of the action potential, was found to interact with perinexal Cx43 but not with ZO-1. This work provides a detailed characterization of the structure of the perinexus at the GJ edge and indicates that one of its potential functions in the heart may be in facilitating conduction of action potential.

Keywords

Connexin43; Duolink; Gap junction; Hemichannel; $Na_v1.5$; Perinexus; Sodium channel

Introduction

The gap junction (GJ) is an aggregate of channels bridging the cytoplasms of adjacent cells. The channels of the GJ allow for passage of small molecules (less than ~1,000 Da) and electrotonic coupling between cells (Liu and Johnson 1999; Palatinus et al. 2012; Severs et al. 2008). Intercellular channels are formed by the interaction of half-channels (called connexons or hemichannels) contributed by each contacting cell (Koval 2006), and connexons are in turn composed of connexin subunit proteins (Evans and Martin 2002). Connexin43 (Cx43) is one of the more commonly expressed connexins in mammalian

gourdier@musc.edu.

tissues, most notably in the ventricular myocardium (Beyer et al. 1987; Delmar and Liang 2012; Desplantez et al. 2007). In the ventricle, Cx43 underpins contraction synchronization by contributing to the mechanism of cell-to-cell propagation of action potential (Kleber and Rudy 2004; Severs et al. 2008).

The Cx43 life cycle begins with cotranslational insertion in the endoplasmic reticulum, after which oligomerization of connexons occurs in the Golgi (Musil and Goodenough 1993). Vesicles containing connexons are then thought to traffic to the plasma membrane along microtubules (Fort et al. 2011), although other work suggests that this pathway is only utilized in specialized conditions (Johnson et al. 2002). In the 2000s, it was shown that new Cx43 channels were predominately added from the edge of the GJ (Gaietta et al. 2002; Lauf et al. 2002). Work by Shaw and colleagues suggested a molecular linkage between delivery of Cx43 vesicles to the membrane and incorporation of connexons into the GJ. These studies showed that Cx43 was trafficked from microtubules directly to N-cadherin associated with GJs via EB1 binding of the p150(Glued)/ dynein/dynactin complex (Shaw et al. 2007).

The Gourdie laboratory has provided evidence that the scaffolding protein zonula occludens-1 (ZO-1) localizes to the edge of GJs, where it regulates addition of new connexons to the plaque (Hunter et al. 2005). Subsequently, it was shown that ZO-1 interaction with undocked connexons in the plasma membrane regulated their transition to GJ intercellular channels (Rhett et al. 2011). In this work, subcellular localization of Cx43/ZO-1 interaction indicated a novel region of plasma membrane surrounding the GJ. This domain was termed the perinexus for its location next to (*peri*-) the junction (-*nexus*). Perinexal Cx43/ZO-1 interaction, in combination with functional assays, suggested that the perinexus functions as a staging area where ZO-1 served to sequester undocked connexons.

The identification of Cx43/ZO-1 interaction localized to the perinexus indicated the presence of Cx43 molecules, but Cx43 in this region was not detectable by standard immunofluorescence (IF). Others have identified putative Cx43 hemichannels in this region (Beahm et al. 2006; Johnson et al. 2012; Lal et al. 1995). Notably, Ross Johnson and colleagues (Johnson et al. 2012) have recently demonstrated that unaggregated connexons reside near newly forming GJs in the formation plaque (FP) by using sophisticated freeze-fracture replica immunogold labeling (FRIL) techniques. Here, we provide the first direct labeling of Cx43 in the perinexus. Using high-sensitivity Duolink labeling of Cx43–Cx43 interactions, we show that Triton X-100-soluble Cx43 localizes and concentrates in the perinexus of mature junctions. Moreover, we provide evidence that the myocardial perinexus may have unique constitutive functions that go beyond the transition of undocked connexons into the GJ. Specifically, we observe that nonjunctional Cx43 interacts with $Na_v1.5$ in the perinexus of cultured cardiomyocytes, indicating a possible role for $Na_v1.5$ in electrical conduction between cells. These results contribute to a viewpoint held by increasing numbers of workers in the field that cell-to-cell propagation of electrical impulse in the heart may be determined by nonelectrotonic mechanisms.

Materials and Methods

Animals

Cardiac myocytes were collected from freshly dissected ventricles of 1- to 2-day-old Sprague Dawley rats. Tissue sections were generated from hearts collected from 12–15-week-old female Sprague Dawley rats. All animal procedures were in accordance with the Medical University of South Carolina IACAUC and NIH Animal Welfare Assurance A3728–01.

Cell Culture

Freshly dissected ventricles were immediately placed in cold HBSS. The ventricles were finely minced and enzymatically dissociated into single cells at 37 °C with gentle rotation. The combined enzymatic fractions were layered onto a Percoll density gradient 1.080/1.060 for myocyte enrichment. Fibroblasts and myocyte layers were collected and washed. Myocytes were plated in M199/EBSS, 5 % NCS, 10 % HS, and antibiotics onto gelatin-coated dishes at 1.3×10^6 cells/35 mm MatTek plate, and 3×10^6 cells/ 60 mm culture plate. Cultures were attached 18–24 h at 37 °C/5 % CO_2. After overnight attachment, cultures were washed twice with DPBS Ca^{2+}/Mg^{2+}. Thereafter, fresh maintenance media was added every 2–3 days, and beating cultures were used for experiments 5 days after plating.

Triton Extraction and Fractionation

NRHMs cultures were subjected to in situ Triton X-100 extraction according to the method of Musil and Goodenough (1991). After the final wash step, plates were fixed and stained as described below, or the remaining cellular material was scraped into 1 ml of Triton X-100 extraction buffer for Western blot analysis. Triton fractionation was carried out as previously described (Rhett et al. 2011). Briefly, cells were lysed in the presence of 1 % Triton X-100 and centrifuged for 50 min at 100,000×g. Supernatants and pellets were separated, and pellets were resolubilized in lysis buffer containing SDS (0.1 % final concentration was used in both fractions).

Immunocytochemistry

Immunofluorescent and Duolink staining was carried out as previously described (Rhett et al. 2011). For Cx43/ZO-1 interaction, primary antibodies used were mouse anti-Cx43 (Millipore MAB3067) and rabbit anti-ZO-1 (Invitrogen 617–300). In these cultures, goat anti-Cx43 (Abcam 87645) was used to detect Cx43 by standard IF. Cx43–Cx43-Duolink was performed both by dual and single primary detection. For dual detection, mouse anti-Cx43 (Millipore MAB3067) and rabbit anti-Cx43 (Sigma C-6219) were used for Duolink with goat anti-Cx43 (Abcam 87645) for detection by standard IF. For single-primary Duolink detection goat anti-Cx43 (Abcam 87645) was used with mouse anti-Cx43 (Millipore MAB3067) for detection by standard IF. For standard IF labeling of NRHMs by Cx43, ZO-1 and $Na_v1.5$ goat anti-Cx43 (Abcam 87645), mouse anti-ZO-1 (Zymed 33–9100), and rabbit anti-$Na_v1.5$ (Alamone ASC-005) were used, respectively. For Cx43/$Na_v1.5$ Duolink labeling mouse anti-Cx43 (Millipore MAB3067) and rabbit anti-$Na_v1.5$ (Alamone ASC-005) were used along with goat anti-Cx43 (Abcam 87645) for

detection of Cx43 by standard IF. For ZO-1/$Na_V1.5$ Duolink labeling mouse anti-ZO-1 (Zymed 33–9100) and rabbit anti-$Na_V1.5$ (Alamone ASC-005) were used along with goat anti-Cx43 (Abcam 87645) for detection of Cx43 by standard IF. Duolink reactions were carried out using appropriate PLA secondary antibodies according to the manufacturers instructions.

Western Blot Testing

For the Triton fractionation/extraction assay proteins were resolved on 10 % SDS-PAGE gels, followed by immuno-blotting for Cx43 with rabbit anti-Cx43 (Sigma C-6219). For $Na_V1.5$ detection, Triton X-100 fractionated NRHM lysates were run on 7 % SDA-PAGE gels, followed by immunoblotting for $Na_V1.5$ (Sigma S0819).

Image Acquisition and Analysis

Confocal images were acquired on a TCS SP5 laser scanning confocal microscope equipped with a 63 ×/1.4 numerical aperture oil objective (Leica, Buffalo Grove, IL). Images were analyzed by ImageJ software (NIH, http://rsbweb.nih.gov/ij/). Measurements were performed on threshold versions of original images, and the same threshold settings were always used within a given experiment.

For Cx43-Duolink density measurements, Cx43 IF images were used to create a selected region of interest encircling GJs, and the integrated density of Cx43-Duolink labeling was measured within the GJ, a region expanded 250 μ_M from the GJ edge, a region expanded 500 μ_M from the GJ edge, and the entire image. The Cx43-Duolink density within each region described in the text was determined by subtraction.

For perinexus width measurements, ellipses were fit to all GJs > μ_M^2 in area (smaller junctions were not much bigger than individual Duolink labels), and the distance was measured from the edge of the GJ plaque to the end of Cx43-Duolink labeling along the major and minor axes. When the perinexus was continuous between two junctions along an axis, measurements could not be made accurately and were not used.

Statistical Analysis

Statistical analysis was carried out by GraphPad Prism software, version 5.0d for Mac OS X (GraphPad, San Diego, CA). Multiple comparisons were made using ANOVA with Tukey's multiple comparison test, and single comparisons used an unpaired *t*-test. *p*-values and numbers are indicated in the text and figure captions.

Results

Cx43 Is Concentrated in the Perinexus of Cardiomyocytes

Recent work with Cx43-expressing HeLa cells and rat epicardial cells has identified a region adjacent to GJs involved in regulating transition of connexons in the membrane to intercellular channels in the GJ plaque (Rhett et al. 2011). This region, termed the perinexus, was defined by Cx43/ZO-1 interaction as visualized by the Duolink assay. Cx43 is the primary isoform of connexin expressed in the working ventricular myocardium (Noorman et

al. 2009), where it plays a critical role in propagation of the action potential (Severs et al. 2008). Therefore, we sought to determine if ventricular cardiomyocytes also displayed a perinexus. Figure 1a shows cultured neonatal rat heart ventricular myocytes (NRHVMs) labeled for Cx43 by standard IF in green, and Cx43/ZO-1 interaction by Duo-link in red. We found that nearly all Cx43-labeled GJ structures coincided with labeling for Cx43/ZO-1 interaction−both within GJ plaques and in the adjacent membrane, indicating that cardiomyocytes also possess a perinexus surrounding Cx43 GJs.

The detection of Cx43/ZO-1 interaction in the perinexus suggests the presence of Cx43 in this region. However, it does not yield information pertaining to the quantity of Cx43 within this region. Attempts have been made to visualize perinexal Cx43 by standard IF (Rhett et al. 2011), but this method is not optimal as it is difficult to determine whether this signal originates from perinexal Cx43 or outof-focus light emanating from the nearby GJ. To avoid this issue, we used Duolink to detect Cx43–Cx43 interaction as a means to resolve Cx43 signals of lower intensity. The rationale for this methodology is that the readout of the Duolink assay is binary−i.e., a Duolink signal is either generated or not depending on whether protein interaction is detected or not−and therefore the number of Duolink signals, and not their intensity, varies with Cx43 concentration within a given region of the cell preparation. Figure 1b depicts neonatal rat heart ventricular myocytes labeled in this manner, with Cx43 labeled by standard IF in green and Cx43–Cx43 interaction by Duolink in red. Duolink signal labeled the GJ, as expected, and also appeared to intensely label the surrounding perinexal membrane, providing direct evidence of Cx43 molecules in the perinexus.

Although inspection of the images labeled with Cx43– Cx43-Duolink clearly show interaction that occurs outside of but near the GJ edge, it is difficult to determine the relative amount of Cx43 in the perinexus by visual inspection as a result of the relatively large size of Duolink signals (~400–500 nm diameter). This effect results in highly concentrated signals originating at the GJ edge but extending as far as 250 nm into the perinexus. Thus, to determine the relative amount of Cx43 in the perinexus, measurements of Duolink signal density were performed in three separate regions of Cx43–Cx43-Duo-link labeled images: the GJ plaque as defined by standard Cx43 IF (innermost cyan line in Fig. 1c), the perinexus limited to the region between 250 and 500 nm from the GJ edge (from the middle cyan line to the outer cyan line), and nonnexal regions of the cell (everything outside of the outer cyan, 500 nm perimeter line). The perinexal Cx43–Cx43-Duolink signal measured in this way could only have originated from outside of the of the GJ plaque edge.

It was found that the density of Cx43-Duolink signal in both the perinexus and nonnexal regions of the cell were significantly lower than within the GJ plaque (Fig. 1c, left). Importantly, the density of signal in the perinexus was approximately 10-fold lower than the GJ−as would be expected based on the IF signal. Additionally, comparison of the perinexus to nonnexus showed a significantly greater concentration of Cx43-Duolink signal in the perinexus (Fig. 1c, right). Despite the above-mentioned limitations of making similar measurements using IF, comparable levels of Cx43 density were ascertained with this method (Online Resource 1). Taken together, these results demonstrate the presence of Cx43

in the perinexus at a much lower concentration than the GJ plaque, but at a substantially higher concentration than the rest of the cell.

The Perinexus Has Variable Shape

Having defined the Cx43 composition of the perinexus, we next sought to analyze the distance that perinexal Cx43 signal extended from the GJ edge. Measurements were performed on images acquired from neonatal rat heart ventricular myocyte cultures by fitting ellipses to GJs, and measuring the distance from the edge of the GJ (labeled by standard Cx43 IF) to the end of contiguous Cx43-Duolink label along major and minor axes of the ellipse (Fig. 2). The method of fitting ellipses and using the major and minor axes as plumb lines along which to measure was done to introduce randomness in where the measurements were taken (i.e., we did not chose the location of the axes) and to ensure that the perinexus width was obtained as near as possible along a line emanating directly outward from the GJ.

It was determined that, after compensating for the size of individual Cx43-Duolink signals, the average width of the perinexus obtained from five separate experiments was 200.4 ± 28.4 nm (mean ± SEM; Fig. 2). We used SEM here to compare means between experiments because it reflects how accurately we know the “true” value of the average perinexus width. The relatively small SEM (i.e., 28.4 nm) indicated that our results were consistent between experiments. However, visual inspection indicated variation in the width of the perinexus for any given GJ (Fig. 2). To this end, we used the standard deviation of all the measurements *within* an experiment to determine the variability between individual perinexus width measurements. The large standard deviation for measurements within an experiment, 313.9 ± 20.4 nm (mean of all experiments ± SEM between experiments; Fig. 2) compared to the ~200 nm perinexus width confirmed our observations.

We did not find any correlation between perinexus width and GJ size as defined by either area or length (R^2 = 0.017 ± 0.015 and 0.033 ± 0.015, respectively), but it was determined that the percentage of measurements for which the perinexus width was recorded as 0 in each experiment was high: 42.4 ± 5.4 %. Furthermore, there was a relatively small percentage of perinexus width measurements over 500 nm (12.5 ± 2.6 %). However, fully 45.1 ± 3.7 % of measurements were between 0 and 500 nm, suggesting that many junctions displayed uniform Cx43-Duolink labeling in the perinexus but that perinexal Cx43 was often distributed in elongated projections from the GJ plaque edge. This could be confirmed by visual inspection of images (Figs. 1b, 2).

Cx43 in the Perinexus Is Nonjunctional

In recent work, correlative biochemical and functional data suggested that at least a portion of Cx43 present in the perinexus was in the form of functional hemichannels (Rhett et al. 2011). To further address the composition of perinexal Cx43 we used in situ Triton X-100 extraction. In this assay, a buffer containing 1 % Triton X-100 was applied to cultured NRHMs with mild agitation, followed by reclamation of the buffer (now containing Triton-soluble portions of the cells) and fixation, staining, and imaging of the remaining Triton-insoluble cellular components left on the culture plate.

To validate the assay, we compared the results of a Triton X-100 detergent extraction to NRHM lysates separated into Triton X-100-soluble (nonjunctional) and -insoluble (junctional) fractions by ultracentrifugation. In this instance of Triton extraction, the cell components remaining on the culture plate were scraped into an equivalent volume of extraction buffer as opposed to being fixed. We compared the two methodologies by Western blot analysis for Cx43 as shown in Fig. 3a. Similar to the results of others in cultured cardiomyocytes (Tence et al. 2012), separation of NRHM lysates by Triton X-100 fractionation resulted in a preponderance of the P1 and P0 phosphoisoforms accumulating in the detergent-soluble fraction, as well as a small amount of the P2 isoform (Fig. 3a, “Triton Soluble” lane).

In contrast, the Triton-insoluble fraction contained a large amount of the P2/P1 isoform, while the P0 isoform was absent (Fig. 3a, “Triton Insoluble” lane). In a similar result, the portion of the cell solubilized by Triton extraction contained all three isoforms of Cx43, but with a much larger amount of the P1 and P2 isoforms than obtained by fractionation (Fig. 3a, “Triton Extracted” lane). The Triton X-100-insoluble cellular remainder also compared favorably to the insoluble fraction obtained by ultracentrifugation in that it appeared to be composed solely of P2/P1 isoforms (Fig. 3a “Triton Unextracted” lane). We concluded from these results that Cx43 in NRHMs separated by the two methodologies yields similar separation of Cx43, with the primary exception that in situ extraction results in a larger amount of P1 and P2 isoforms segregating into the Triton X-100-soluble extract, suggesting that some of the junctional Cx43 on the culture plate was solubilized.

The fixed, stained, and imaged component of a Triton X-100-extracted NRHM culture is shown in Fig. 3b, “Extraction.” As controls, NRHMs were fixed, labeled, and imaged without any extraction procedure (Fig. 3b, “Control”) or after a mock extraction in which no Triton X-100 was added to the extraction buffer (Fig. 3b, “Mock”). The preparations were labeled for Cx43 both by standard IF in green and Duolink in red. By visual inspection, it appeared that Cx43-Duolink label colocalized with GJs, and extended well into the perinexal region in the controls (Fig. 3b, “Control” and “Mock”), similar to the results presented in Fig. 1. In contrast, the unextracted cellular remains of cultures exposed to Triton X-100 displayed little perinexal Cx43-Duolink label, indicating that Cx43 in the perinexus is Triton soluble (Fig. 3b, “Extraction”).

To confirm this result, we measured Cx43-Duolink density (as described above) in the three treatments. We found that Cx43 was significantly reduced in the perinexus of Triton-extracted NRHMs when compared to the control (Fig. 3c). Importantly, the Triton-solubilized component could be demonstrated by Western blot analysis to contain Cx43 in a similar banding profile to that of the “Triton Soluble” fraction of ultracentrifuged lysates (cf. Western blot analysis in Fig. 3c to “Triton Soluble” lane in Fig. 3a), while the reclaimed buffer from mock extracted cultures contained no detectable Cx43. These results demonstrate that Cx43 in the perinexus is Triton X-100 soluble−i.e., nonjunctional−and therefore potentially in the form of undocked connexons/hemichannels. Moreover, the loss of Cx43 signals from around the GJ edge after detergent solubilization provided evidence that these signals were not accounted for by out-of-focus fluorescence and that the perinexus is a membrane structure with physical properties that distinguish it from the GJ proper.

Cx43 Interacts with $Na_v1.5$ in the Perinexus

Our next goal was to investigate other Cx43 protein partners and their relationship to the perinexus. Of particular interest was the voltage gated sodium channel $Na_v1.5$ as a result of its role in generating the cardiac action potential. It has previously been shown to localize to the intercalated disc (Cohen 1996; Colussi et al. 2010; Maier et al. 2002; Malhotra et al. 2004; Noorman et al. 2008; Petitprez et al. 2011; Stein et al. 2009) and interact with Cx43 (Malhotra et al. 2004). We first used a standard IF labeling and confocal imaging protocol to study the codistribution of the two proteins in NRHM cultures. Cell preparations were labeled with Cx43 in green, ZO-1 in red, and $Na_v1.5$ in blue (Fig. 4a). As has been previously described, ZO-1 localized to the GJ edge and surrounding area (Hunter et al. 2005; Hunter and Gourdie 2008; Palatinus et al. 2011; Zhu et al. 2005). In a result confirming that described by Yoram Rudy and coworkers (Kucera et al. 2002), we found a high degree of overlap between the Cx43 and $Na_v1.5$ signals (Fig. 4a). We further investigated the relationship between Cx43 and $Na_v1.5$ by performing a Duolink assay for Cx43/$Na_v1.5$ interaction. This determined that the Cx43/$Na_v1.5$ Duolink label closely resembled that of Cx43/ZO-1 interaction (cf. Figs. 4b, Fig. 1a), with Cx43/$Na_v1.5$ Duolink signal overlapping with Cx43 GJs labeled by standard IF, and more frequently localizing to the perinexus region (Fig. 4b). Because of the similarities between Cx43 and $Na_v1.5$ codistribution with ZO-1, and the resemblance of the Cx43/ZO-1 interaction pattern to that of Cx43/$Na_v1.5$, we also labeled NRHM cultures for ZO-1/$Na_v1.5$ interaction (Fig. 4c). Very few Duolink signals were generated with this protocol, indicating that ZO-1 and $Na_v1.5$ have little, if any, interaction in agreement with Abriel and coworkers (Petitprez et al. 2011).

The biochemical relationship between Cx43 and $Na_v1.5$ was addressed by Triton X-100 fractionation of NRHM lysates, followed by Western blot analysis of $Na_v1.5$ (Fig. 4d). For comparison, the Triton fractionated and extracted samples from Fig. 2 have been included. It was found that $Na_v1.5$ almost exclusively segregated into the Triton-soluble pool (Fig. 4d). On the basis of these results, we concluded that $Na_v1.5$ associates with nonjunctional Cx43 (connexons/hemichannels) in the perinexus.

Discussion

The purpose of this study was to characterize the composition and structure of the cardiomyocyte perinexus. This study provides the first comprehensive depiction of the location, extent, and quantity of Cx43 in this specialized region of membrane. The canonical pathway for GJ accretion at the GJ edge was first introduced over 10 years ago (Gaietta et al. 2002; Lauf et al. 2002). In and of itself, this mechanism of GJ aggregation suggests the presence of Cx43 in the surrounding membrane. Our measurements describe a region surrounding the GJ plaque that contains nonuniformly distributed Cx43 molecules at a higher concentration than other nonjunctional regions of the cell.

Comparison of Confocal Cx43-Duolink Imaging to GJs Imaged by Electron Microscopy of Freeze-fracture Replicas

In freeze-fracture studies, Johnson et al. (2012) have reported immunogold detection of unaggregated, nonjunctional Cx43 particles (presumptive connexons) near GJs in the FP. At first glance, these data suggest that the FP and perinexus may be the same structure. However, several important distinctions must be made.

First, in Johnson's seminal work on the FP, the initiation of GJ formation is studied in a model system using reaggregated cells (Johnson et al. 1974). Electron microscopy of freeze-fracture replicas from cells within the first hour after reaggregation revealed the FP as a prominent structure. Over that time period, 9–11 nm intramembraneous particles (IMPs), presumptive connexin channels, displayed first as unaggregated, then “clustered” (i.e., associated but not packed in hexagonal arrays), and finally as GJ aggregates within the FP. However, at later time points (2–3 h), the FP reduced to a narrow, particle-free halo around the junction (Johnson et al. 1974). In contrast, the cardiomyocytes we labeled were cultured for nearly a week before fixation, and we observed perinexus widths as great as ~2.5 μ_M−as defined by the *presence* of Cx43.

Differentiation of the FP and perinexus on these criteria is supported by a detailed comparison of Cx36 GJs imaged by confocal vs. FRIL. Kamasawa et al. (2006) showed that by enhancing the “dark output” (i.e., low intensity Cx36 IF signals) of confocal images, smaller GJ punctae corresponding to string and ribbon GJs become visible. Similarly, we find that measurement of low-intensity IF signal in the perinexus indicates the presence of Cx43 in that region of the cell at a higher concentration than nonjunctional regions of the cell (Online Resource 1). Corroboration of this result by Duolink confirms the findings of Kamasawa et al. on the limits of light microscopy. In addition, Kamasawa et al. show that confocal microscopy of Cx36 GJs overestimates the size of those junctions as compared to measurements made by electron microscopy of freeze-fracture replicas. If this relationship holds true for Cx43, then this would suggest that the ~200 nm average distance that we measure Cx43-Duolink signal emanating from the GJ edge actually underestimates the extent of the perinexus−again suggesting that in mature junctions, the perinexus extends far beyond the FP.

Second, in remarkable stereoscopic FRIL images of Cx36 in goldfish Mauthner cells, Flores et al. (2012) showed vesicles inserting putative hemichannels near mature GJs. Furthermore, “tall” IMPs in P-face images and immunogold labeling of Cx36 in E-face images of clustered particles adjacent to GJs suggest docking of connexons just before accretion in the GJ. Similar results were obtained by Johnson et al. (2012) for Cx43 in the FP of immature junctions. These data support a role for the perinexus in the constitutive transition of hemichannels to GJ intercellular channels in mature junctions that has been previously proposed (Rhett and Gourdie 2012; Rhett et al. 2011), and this is underscored by our finding that perinexal Cx43 is nonjunctional as defined by Triton X-100 solubility (Fig. 3).

Finally, one defining feature of the FP is the exclusion of IMPs other than the 9–11 nm connexin channels (Johnson et al. 1974, 2012). In contrast, we conceive of the perinexus not only as the region of membrane surrounding the GJ, but as a complex assemblage of

channels (at least Cx43 and $Na_v1.5$ [Rhett and Gourdie 2012; Rhett et al. 2011]; Figs. 1, 4), scaffolding proteins (ZO-1 [Hunter et al. 2005; Rhett et al. 2011]; Fig. 1), junctional molecules (N-cadherin [Hunter and Gourdie 2008; and unpublished data]), and cytoskeletal elements (actin [Rhett and Gourdie 2012; Rhett et al. 2011; and unpublished data]). We envisage the perinexus as a constitutive structure, albeit dynamic, with ongoing homeostatic functions including HC regulation, conduction, and GJ dynamics. The FP, as conceived by Johnson et al. (1974, 2002, 2012), seems to be a more transient construct that serves largely during the establishment and building of a GJ.

Despite these differences, it is undeniable that there are parallels between the FP and perinexus. Both are involved in the transition to and aggregation of GJ channels. During the building phase of immature GJs, the perinexus and FP are likely to be indistinguishable. One possibility that arises is that the FP is a temporal and spatial subset of the perinexus. Another, and perhaps more intriguing, possibility is that the perinexus is an exapted derivative of the FP− where the molecular machinery delivering connexons to the edge of the plaque may have assumed new functions and elaborated structure during evolution.

Interpretation of Perinexus Structure as Determined by Cx43-Duolink

Importantly, we did not find Cx43-Duolink labeling in the perinexus to be uniform. Rather, the labeling tended to cluster or shift to subdomains of the perinexus (Figs. 1b, 2). One possible explanation involves the size and efficiency of Duolink labeling. First, Duolink signals are limited in their ability to optically resolve structures by their size (up to 1 μm in diameter [Clausson et al. 2011; Jarvius et al. 2006]; 400–500 nm diameter in our hands). For this reason, it was impossible to precisely determine the exact density, extent, and shape of the perinexus. For example, we limited the region analyzed for Cx43 density in the perinexus to exclude the region 0–250 nm from the GJ edge in order to account for the 250 nm radius of a Duolink signal. In the future, a technique such as stimulated emission depletion microscopy could provide approaches to increasing resolution of perinexal Cx43.

In addition, the exact fraction of interaction events that Duolink labels varies from preparation to preparation, cell to cell, and probably even subcellular domain to subcellular domain (Clausson et al. 2011). Because of this it is difficult to be sure that variation in the shape of Cx43-Duolink labeling in the perinexus is a result of genuine clustering of Cx43 within the perinexus, steric hindrance of the ligation or PCR reaction by Cx43 molecular partners, an unknown feature of subcellular structure, or stochasticity inherent to Duolink labeling. However, these caveats being raised, the high consistency of labeling from experiment to experiment suggests that the Cx43-Duolink labeling pattern does reflect the actual location of Cx43 molecules in the perinexus. Moreover, the ability of the Duolink technology to provide strong signals from low density concentrations of Cx43 may be helpful in resolving areas of debate such as whether Cx43 is associated with subcellular structures such as microtubules and mitochondria (Rodriguez-Sinovas et al. 2006).

Given that the Cx43-Duolink labeling pattern authentically mirrors the nature of Cx43 in the perinexus, a biological explanation for this phenomenon could potentially be rooted in the mechanism of connexon delivery to the cell surface. It has been observed that N-cadherin labeling/ area composita is/are coincident with the GJ edge (Delmar and Liang 2012;

Palatinus et al. 2011). Shaw et al. (2007) reported that connexons are delivered along microtubules linked to adherens junctions via EB1 interaction with the p150(Glued)/dynein/dynactin complex. Here, we observed large extensions of the perinexus, sometimes extending as much as 2 μM from the plaque edge. Putting these ideas together, the possibility is suggested that the perinexus serves as the site of delivery of new, undocked connexons to the plasma membrane. This hypothesis is supported by the above-mentioned work of Flores et al. (2012), in which vesicles inserting putative hemichannels adjacent to GJs were observed.

This exciting possibility leads to interesting questions about the molecular mechanics of GJ accretion. For example, phosphorylation on S365 and S325/S328/S330 have been associated with the incorporation of Cx43 into GJ plaques (Lampe et al. 2006; Solan and Lampe 2007; Solan et al. 2007). Future high-resolution/sensitivity studies of the subcellular localization of these Cx43 phosphoisoforms could yield insights into the role of phosphorylation state in GJ assembly.

Another possible interpretation of our observation of Cx43 concentrated in the perinexus is implicated by the work of Shaw and colleagues. Smyth et al. (2012) reported that actin also participates in anterograde trafficking of Cx43 to GJs in cardiomyocytes. They propose that vesicles containing Cx43 and associated with actin fibers might accumulate in the submembrane near GJs, awaiting transport to the GJ by transfer to the microtubule system. Therefore, it is possible to interpret the data provided in the present investigation as Cx43 in "intracellular reserves." Given that multiple lines of evidence support the existence of functional hemichannels (Li et al. 1996; Quist et al. 2000; Rhett et al. 2011; Saez et al. 2003; Thompson et al. 2006), it is unlikely that Cx43 in or near the plasma membrane only exists in either actinsequestered vesicles or the GJ plaque. Therefore, a combination of models in which perinexal Cx43 represents an accumulation of undocked connexons both in intracellular vesicles and in the plasma membrane is more likely.

Finally, new work on the effects of G protein–coupled receptor agonists has shed light on the role of Cx43/ZO-1 interaction. Past studies have shown that endothelin-1 (ET-1) can regulate both GJ intercellular communication (GJIC; van Zeijl et al. 2007) and internalization (Baker et al. 2008). Importantly, both these studies showed a critical role for Cx43/ZO-1 interaction in mediating the effects of ET-1. In a detailed study, Tence et al. (2012) recently demonstrated in cultured astrocytes that Cx43/ZO-1 interaction increased and GJIC decreased in response to ET-1, in agreement with the previous reports. Notably, they also found that the pool of Cx43 interacting with ZO-1 in response to ET-1 became Triton X-100 soluble. Because Cx43/ZO-1 interaction is detected in the perinexus (Fig. 1a; Rhett et al. 2011) and the perinexus is likely to be composed of undocked connexons, it is interesting to speculate that the perinexus is involved in GJ internalization and reductions in GJIC associated with ET-1.

The Perinexus Indicates Noncanonical Roles for Cx43

In addition to trafficking, other roles for perinexal Cx43 are indicated. For example, the perinexus may represent a platform to regulate the balance between intercellular communication and hemichannel-mediated membrane permeability (Rhett et al. 2011). A

means of rapid control over intercellular communication has obvious implications for excitable tissues, but the ability to quickly enhance or reduce hemichannel function could give cells the ability to regulate GJ-mediated adhesivity, volume (Quist et al. 2000), ATP signaling (Yuan et al. 2012), or cell death (Decrock et al. 2009; Shintani-Ishida et al. 2007), to name a few examples.

In addition to providing subcellular Cx43 localization in previously unparalleled detail, we show that Cx43 interacts with $Na_v1.5$ in the perinexus of cardiomyocytes (Fig. 4b). We also demonstrate that $Na_v1.5$ has, at best, a low level of interaction with ZO-1. The few Duolink labels that we did observe rarely coincided with the perinexus. These data suggest that there may be a complex pattern of association and segregation between molecular complexes in the perinexus. Indeed, if Cx43/ZO-1 interaction occurs in the perinexus (Fig. 1a), and if Cx43/$Na_v1.5$ interaction occurs in the perinexus but ZO-1/$Na_v1.5$ interaction does not, it suggests that Cx43 interaction with $Na_v1.5$ is mutually exclusive with Cx43/ZO-1 interaction.

Importantly, our finding that $Na_v1.5$ localizes to both the perinexus (Fig. 4b) and the GJ itself (Fig. 4a) places it in a region of close apposition between two cell membranes. Intriguingly, this nonjunctional location at the GJ edge would uniquely position sodium channels for participation nonelectrotonic mechanisms of propagation electrical excitation in the heart. Mori et al. (2008) have demonstrated in a 3-D electrodiffusion model of conduction that even in the absence of GJ coupling, conduction can occur between cells when their membranes are ~2 to 7 nm apart via an electric field mechanism. Whether or not $Na_v1.5$ participates in coupling across narrow clefts in extracellular space occurring at GJs is not addressed by our data. Nonetheless, there is mounting evidence that Cx43 alone is insufficient and that both Cx43 and $Na_v1.5$ are necessary in the mechanism of cell-to-cell transmission of action potential (Gutstein et al. 2001; Jansen et al. 2012; Lin et al. 2011). Moreover, it has been demonstrated that increasing interstitial volume reduces conduction velocity on a time-scale incompatible with GJ remodeling (Veeraraghavan et al. 2012). Sites of high concentration of depolarizing currents and close membrane–membrane apposition raise the potential for electric field transmission at the GJ edge as an auxiliary conduction pathway.

Conclusion

The perinexus is a region of membrane involved in the regulation of GJIC and membrane permeability (Rhett et al. 2011). The data presented herein provide the first direct measurement of concentrated Cx43 in the perinexus, in the form of undocked connexons, suggesting the possibilities that this specialized zone of the plasma membrane has functions in GJ assembly, hemichannel function, and signaling. In particular, the data we present here on Cx43/ $Na_v1.5$ interaction in the perinexus indicates that this specialized domain of membrane could have assignments in impulse conduction. As such, the perinexus represents a new target for amelioration of arrhythmia via its potential role in novel pathways for electrical coupling between myocytes in the heart.

Supplementary Material

Refer to Web version on PubMed Central for supplementary material.

Acknowledgments

Acknowledgments This work was supported in part by grants from the National Institutes of Heath (RO1 HL56728-10A2 to RGG, RO11DE019355-1 RGG subcontract, F30 HL095320-01 RGG mentor, and 5P20RR016434-07 RGG mentor), and an AHA Grant-in-Aid (RGG).

References

Baker SM, Kim N, Gumpert AM, Segretain D, Falk MM. Acute internalization of gap junctions in vascular endothelial cells in response to inflammatory mediator-induced G-protein coupled receptor activation. FEBS Lett. 2008; 582:4039–4046. [PubMed: 18992245]

Beahm DL, Oshima A, Gaietta GM, Hand GM, Smock AE, Zucker SN, Toloue MM, Chandrasekhar A, Nicholson BJ, Sosinsky GE. Mutation of a conserved threonine in the third trans-membrane helix of alpha- and beta-connexins creates a dominant-negative closed gap junction channel. J Biol Chem. 2006; 281:7994–8009. [PubMed: 16407179]

Beyer EC, Paul DL, Goodenough DA. Connexin43: a protein from rat heart homologous to a gap junction protein from liver. J Cell Biol. 1987; 105:2621–2629. [PubMed: 2826492]

Clausson CM, Allalou A, Weibrecht I, Mahmoudi S, Farnebo M, Landegren U, Wahlby C, Soderberg O. Increasing the dynamic range of in situ PLA. Nat Methods. 2011; 8:892–893. [PubMed: 22036742]

Cohen SA. Immunocytochemical localization of rH1 sodium channel in adult rat heart atria and ventricle. Presence in terminal intercalated disks. Circulation. 1996; 94:3083–3086. [PubMed: 8989112]

Colussi C, Berni R, Rosati J, Straino S, Vitale S, Spallotta F, Baruffi S, Bocchi L, Delucchi F, Rossi S, Savi M, Rotili D, Quaini F, Macchi E, Stilli D, Musso E, Mai A, Gaetano C, Capogrossi MC. The histone deacetylase inhibitor suberoylanilide hydroxamic acid reduces cardiac arrhythmias in dystrophic mice. Cardiovasc Res. 2010; 87:73–82. [PubMed: 20164117]

Decrock E, De Vuyst E, Vinken M, Van Moorhem M, Vranckx K, Wang N, Van Laeken L, De Bock M, DÕHerde K, Lai CP, Rogiers V, Evans WH, Naus CC, Leybaert L. Connexin 43 hemichannels contribute to the propagation of apoptotic cell death in a rat C6 glioma cell model. Cell Death Differ. 2009; 16:151–163. [PubMed: 18820645]

Delmar M, Liang FX. Connexin43 and the regulation of intercalated disc function. Heart Rhythm. 2012; 9:835–838. [PubMed: 22056332]

Desplantez T, Dupont E, Severs NJ, Weingart R. Gap junction channels and cardiac impulse propagation. J Membr Biol. 2007; 218:13–28. [PubMed: 17661127]

Evans WH, Martin PE. Gap junctions: structure and function (review). Mol Membr Biol. 2002; 19:121–136. [PubMed: 12126230]

Flores CE, Nannapaneni S, Davidson KG, Yasumura T, Bennett MV, Rash JE, Pereda AE. Trafficking of gap junction channels at a vertebrate electrical synapse in vivo. Proc Natl Acad Sci USA. 2012; 109:E573–E582. [PubMed: 22323580]

Fort AG, Murray JW, Dandachi N, Davidson MW, Dermietzel R, Wolkoff AW, Spray DC. In vitro motility of liver connexin vesicles along microtubules utilizes kinesin motors. J Biol Chem. 2011; 286:22875–22885. [PubMed: 21536677]

Gaietta G, Deerinck TJ, Adams SR, Bouwer J, Tour O, Laird DW, Sosinsky GE, Tsien RY, Ellisman MH. Multicolor and electron microscopic imaging of connexin trafficking. Science. 2002; 296:503–507. [PubMed: 11964472]

Gutstein DE, Morley GE, Tamaddon H, Vaidya D, Schneider MD, Chen J, Chien KR, Stuhlmann H, Fishman GI. Conduction slowing and sudden arrhythmic death in mice with cardiac-restricted inactivation of connexin43. Circ Res. 2001; 88:333–339. [PubMed: 11179202]

Hunter AW, Gourdie RG. The second PDZ domain of zonula occludens-1 is dispensable for targeting to connexin 43 gap junctions. Cell Commun Adhes. 2008; 15:55–63. [PubMed: 18649178]

Hunter AW, Barker RJ, Zhu C, Gourdie RG. Zonula occludens-1 alters connexin43 gap junction size and organization by influencing channel accretion. Mol Biol Cell. 2005; 16:5686–5698. [PubMed: 16195341]

Jansen JA, Noorman M, Musa H, Stein M, de Jong S, van der Nagel R, Hund TJ, Mohler PJ, Vos MA, van Veen TA, de Bakker JM, Delmar M, van Rijen HV. Reduced heterogeneous expression of Cx43 results in decreased Nav1.5 Expression and reduced sodium current which accounts for arrhythmia vulnerability in conditional Cx43 knockout mice. Heart Rhythm. 2012; 9:600–607. [PubMed: 22100711]

Jarvius J, Melin J, Goransson J, Stenberg J, Fredriksson S, Gonzalez-Rey C, Bertilsson S, Nilsson M. Digital quantification using amplified single-molecule detection. Nat Methods. 2006; 3:725–727. [PubMed: 16929318]

Johnson R, Hammer M, Sheridan J, Revel JP. Gap junction formation between reaggregated Novikoff hepatoma cells. Proc Natl Acad Sci USA. 1974; 71:4536–4540. [PubMed: 4373716]

Johnson RG, Meyer RA, Li XR, Preus DM, Tan L, Grunenwald H, Paulson AF, Laird DW, Sheridan JD. Gap junctions assemble in the presence of cytoskeletal inhibitors, but enhanced assembly requires microtubules. Exp Cell Res. 2002; 275:67–80. [PubMed: 11925106]

Johnson RG, Reynhout JK, TenBroek EM, Quade BJ, Yasumura T, Davidson KG, Sheridan JD, Rash JE. Gap junction assembly: roles for the formation plaque and regulation by the C-terminus of connexin43. Mol Biol Cell. 2012; 23:71–86. [PubMed: 22049024]

Kamasawa N, Furman CS, Davidson KG, Sampson JA, Magnie AR, Gebhardt BR, Kamasawa M, Yasumura T, Zumbrunnen JR, Pickard GE, Nagy JI, Rash JE. Abundance and ultra-structural diversity of neuronal gap junctions in the OFF and ON sublaminae of the inner plexiform layer of rat and mouse retina. Neuroscience. 2006; 142:1093–1117. [PubMed: 17010526]

Kleber AG, Rudy Y. Basic mechanisms of cardiac impulse propagation and associated arrhythmias. Physiol Rev. 2004; 84:431–488. [PubMed: 15044680]

Koval M. Pathways and control of connexin oligomerization. Trends Cell Biol. 2006; 16:159–166. [PubMed: 16490353]

Kucera JP, Rohr S, Rudy Y. Localization of sodium channels in intercalated disks modulates cardiac conduction. Circ Res. 2002; 91:1176–1182. [PubMed: 12480819]

Lal R, John SA, Laird DW, Arnsdorf MF. Heart gap junction preparations reveal hemiplaques by atomic force microscopy. Am J Physiol. 1995; 268:C968–C977. [PubMed: 7733245]

Lampe PD, Cooper CD, King TJ, Burt JM. Analysis of connexin43 phosphorylated at S325, S328 and S330 in normoxic and ischemic heart. J Cell Sci. 2006; 119:3435–3442. [PubMed: 16882687]

Lauf U, Giepmans BN, Lopez P, Braconnot S, Chen SC, Falk MM. Dynamic trafficking and delivery of connexons to the plasma membrane and accretion to gap junctions in living cells. Proc Natl Acad Sci USA. 2002; 99:10446–10451. [PubMed: 12149451]

Li H, Liu TF, Lazrak A, Peracchia C, Goldberg GS, Lampe PD, Johnson RG. Properties and regulation of gap junctional hemichannels in the plasma membranes of cultured cells. J Cell Biol. 1996; 134:1019–1030. [PubMed: 8769424]

Lin X, Liu N, Lu J, Zhang J, Anumonwo JM, Isom LL, Fishman GI, Delmar M. Subcellular heterogeneity of sodium current properties in adult cardiac ventricular myocytes. Heart Rhythm. 2011; 8:1923–1930. [PubMed: 21767519]

Liu TF, Johnson RG. Effects of TPA on dye transfer and dye leakage in fibroblasts transfected with a connexin 43 mutation at ser368. Methods Find Exp Clin Pharmacol. 1999; 21:387–390. [PubMed: 10445229]

Maier SK, Westenbroek RE, Schenkman KA, Feigl EO, Scheuer T, Catterall WA. An unexpected role for brain-type sodium channels in coupling of cell surface depolarization to contraction in the heart. Proc Natl Acad Sci USA. 2002; 99:4073–4078. [PubMed: 11891345]

Malhotra JD, Thyagarajan V, Chen C, Isom LL. Tyrosinephosphorylated and nonphosphorylated sodium channel beta1 subunits are differentially localized in cardiac myocytes. J Biol Chem. 2004; 279:40748–40754. [PubMed: 15272007]

Mori Y, Fishman GI, Peskin CS. Ephaptic conduction in a cardiac strand model with 3D electrodiffusion. Proc Natl Acad Sci USA. 2008; 105:6463–6468. [PubMed: 18434544]

Musil LS, Goodenough DA. Biochemical analysis of connexin43 intracellular transport, phosphorylation, and assembly into gap junctional plaques. J Cell Biol. 1991; 115:1357–1374. [PubMed: 1659577]

Musil LS, Goodenough DA. Multisubunit assembly of an integral plasma membrane channel protein, gap junction connexin43, occurs after exit from the ER. Cell. 1993; 74:1065–1077. [PubMed: 7691412]

Noorman M, van Rijen HV, van Veen TA, de Bakker JM, Stein M. Differences in distribution of fibrosis in the ventricles underlie dominant arrhythmia vulnerability of the right ventricle in senescent mice. Neth Heart J. 2008; 16:356–358. [PubMed: 18958260]

Noorman M, van der Heyden MA, van Veen TA, Cox MG, Hauer RN, de Bakker JM, van Rijen HV. Cardiac cell–cell junctions in health and disease: electrical versus mechanical coupling. J Mol Cell Cardiol. 2009; 47:23–31. [PubMed: 19344726]

Palatinus JA, OÕQuinn MP, Barker RJ, Harris BS, Jourdan J, Gourdie RG. ZO-1 determines adherens and gap junction localization at intercalated disks. Am J Physiol Heart Circ Physiol. 2011; 300:H583–H594. [PubMed: 21131473]

Palatinus JA, Rhett JM, Gourdie RG. The connexin43 carboxyl terminus and cardiac gap junction organization. Biochim Biophys Acta. 2012; 1818:1831–1843. [PubMed: 21856279]

Petitprez S, Zmoos AF, Ogrodnik J, Balse E, Raad N, El-Haou S, Albesa M, Bittihn P, Luther S, Lehnart SE, Hatem SN, Coulombe A, Abriel H. SAP97 and dystrophin macro-molecular complexes determine two pools of cardiac sodium channels Nav1.5 in cardiomyocytes. Circ Res. 2011; 108:294–304. [PubMed: 21164104]

Quist AP, Rhee SK, Lin H, Lal R. Physiological role of gapjunctional hemichannels. Extracellular calcium-dependent isosmotic volume regulation. J Cell Biol. 2000; 148:1063–1074. [PubMed: 10704454]

Rhett JM, Gourdie RG. The perinexus: a new feature of Cx43 gap junction organization. Heart Rhythm. 2012; 9:619–623. [PubMed: 21978964]

Rhett JM, Jourdan J, Gourdie RG. Connexin 43 connexon to gap junction transition is regulated by zonula occludens-1. Mol Biol Cell. 2011; 22:1516–1528. [PubMed: 21411628]

Rodriguez-Sinovas A, Boengler K, Cabestrero A, Gres P, Morente M, Ruiz-Meana M, Konietzka I, Miro E, Totzeck A, Heusch G, Schulz R, Garcia-Dorado D. Translocation of connexin 43 to the inner mitochondrial membrane of cardiomyocytes through the heat shock protein 90-dependent TOM pathway and its importance for cardioprotection. Circ Res. 2006; 99:93–101. [PubMed: 16741159]

Saez JC, Contreras JE, Bukauskas FF, Retamal MA, Bennett MV. Gap junction hemichannels in astrocytes of the CNS. Acta Physiol Scand. 2003; 179:9–22. [PubMed: 12940934]

Severs NJ, Bruce AF, Dupont E, Rothery S. Remodelling of gap junctions and connexin expression in diseased myocardium. Cardiovasc Res. 2008; 80:9–19. [PubMed: 18519446]

Shaw RM, Fay AJ, Puthenveedu MA, von Zastrow M, Jan YN, Jan LY. Microtubule plus-end-tracking proteins target gap junctions directly from the cell interior to adherens junctions. Cell. 2007; 128:547–560. [PubMed: 17289573]

Shintani-Ishida K, Uemura K, Yoshida K. Hemichannels in cardiomyocytes open transiently during ischemia and contribute to reperfusion injury following brief ischemia. Am J Physiol Heart Circ Physiol. 2007; 293:H1714–H1720. [PubMed: 17557925]

Smyth JW, Vogan JM, Buch PJ, Zhang SS, Fong TS, Hong TT, Shaw RM. Actin cytoskeleton rest stops regulate anterograde traffic of connexin 43 vesicles to the plasma membrane. Circ Res. 2012; 110:978–989. [PubMed: 22328533]

Solan JL, Lampe PD. Key connexin 43 phosphorylation events regulate the gap junction life cycle. J Membr Biol. 2007; 217:35–41. [PubMed: 17629739]

Solan JL, Marquez-Rosado L, Sorgen PL, Thornton PJ, Gafken PR, Lampe PD. Phosphorylation at S365 is a gatekeeper event that changes the structure of Cx43 and prevents down-regulation by PKC. J Cell Biol. 2007; 179:1301–1309. [PubMed: 18086922]

Stein M, van Veen TA, Remme CA, Boulaksil M, Noorman M, van Stuijvenberg L, van der Nagel R, Bezzina CR, Hauer RN, de Bakker JM, van Rijen HV. Combined reduction of intercellular coupling and membrane excitability differentially affects transverse and longitudinal cardiac conduction. Cardiovasc Res. 2009; 83:52–60. [PubMed: 19389723]

Tence M, Ezan P, Amigou E, Giaume C. Increased interaction of connexin43 with zonula occludens-1 during inhibition of gap junctions by G protein-coupled receptor agonists. Cell Signal. 2012; 24:86–98. [PubMed: 21872657]

Thompson RJ, Zhou N, MacVicar BA. Ischemia opens neuronal gap junction hemichannels. Science. 2006; 312:924–927. [PubMed: 16690868]

van Zeijl L, Ponsioen B, Giepmans BN, Ariaens A, Postma FR, Varnai P, Balla T, Divecha N, Jalink K, Moolenaar WH. Regulation of connexin43 gap junctional communication by phosphatidylinositol 4,5-bisphosphate. J Cell Biol. 2007; 177:881–891. [PubMed: 17535964]

Veeraraghavan R, Salama ME, Poelzing S. Interstitial volume modulates the conduction velocity–gap junction relationship. Am J Physiol Heart Circ Physiol. 2012; 302:H278–H286. [PubMed: 22021331]

Yuan D, Wang Q, Wu D, Yu M, Zhang S, Li L, Tao L, Harris AL. Monocyte–endothelial adhesion is modulated by Cx43-stimulated ATP release from monocytes. Biochem Biophys Res Commun. 2012; 420:536–541. [PubMed: 22446325]

Zhu C, Barker RJ, Hunter AW, Zhang Y, Jourdan J, Gourdie RG. Quantitative analysis of ZO-1 colocalization with Cx43 gap junction plaques in cultures of rat neonatal cardiomyocytes. Microsc Microanal. 2005; 11:244–248. [PubMed: 16060977]

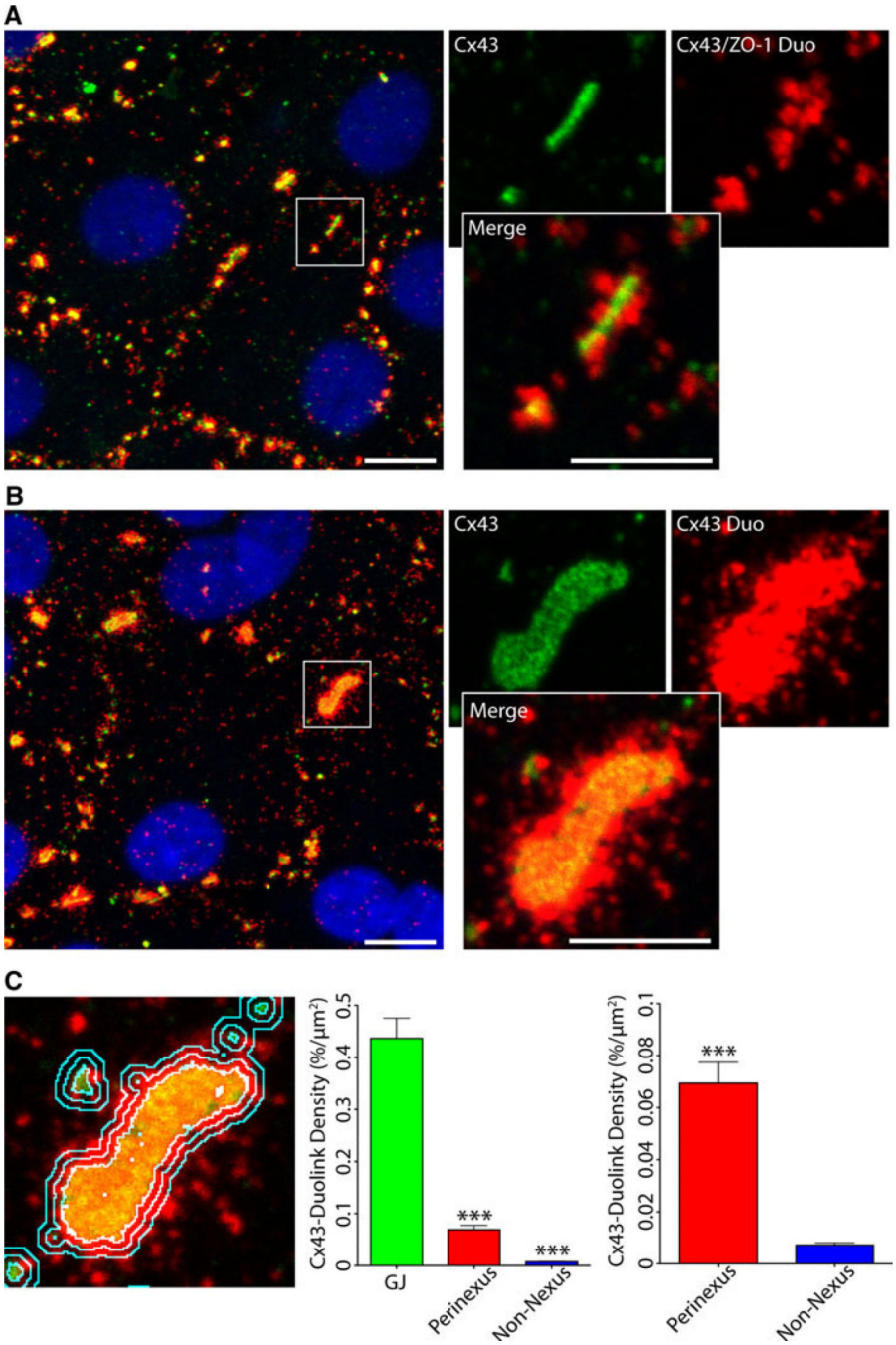

Fig. 1.

NHRMs display a perinexus that contains concentrated Cx43 molecules. **a** Cultured NRHMs were labeled for Cx43 by standard IF (*green*), Cx43/ZO-1 interaction by Duolink (*red*), and the nucleus (*blue*). Note the preponderance of Duolink spots adjacent to the GJ plaque. **b** Cx43 is labeled in the perinexus by high-sensitivity Duolink. Cx43 is labeled both by standard IF (*green*) and by Duolink (*red*). The nucleus is labeled in *blue*. **c** Analysis of Duolink-labeled Cx43. The image shows the same GJ expanded in (**b**) with cyan lines demarcating the GJ perimeter (*innermost line*), and 250 and 500 nm from the perimeter

(*middle* and *outer* lines, respectively). The graphs show averaged measurements of Cx43-Duolink density within the *innermost line* (GJ), between the *middle* and *outer lines* (Perinexus), and exterior to the *outermost line* (Non-Nexus). The *left* graph compares all three regions; the *right* graph limits the comparison to the perinexus and nonnexal regions (***$p < 0.001$ and ****$p < 0.0001$; $n = 5$). *Error bars* represent SEM; *scale bars* represent 10 μm in large images, and 5 μm in expanded images

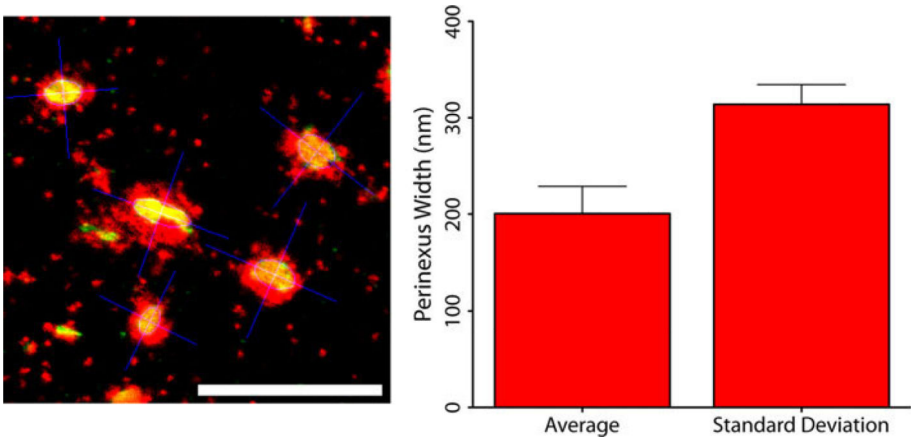

Fig. 2.

The perinexus has a distinct shape. Confocal image of typical GJs and perinexi from cultured NRHMs. Cx43 is labeled by standard IF in *green*, Duolink in *red*, and fitted ellipses with major and minor axes are in *blue* (*left*). *Scale bar* 10 μm. The graph at *right* shows the perinexus width, averaged over 5 experiments, and the standard deviation for individual measurements within each experiment. *Error bars* represent SEM

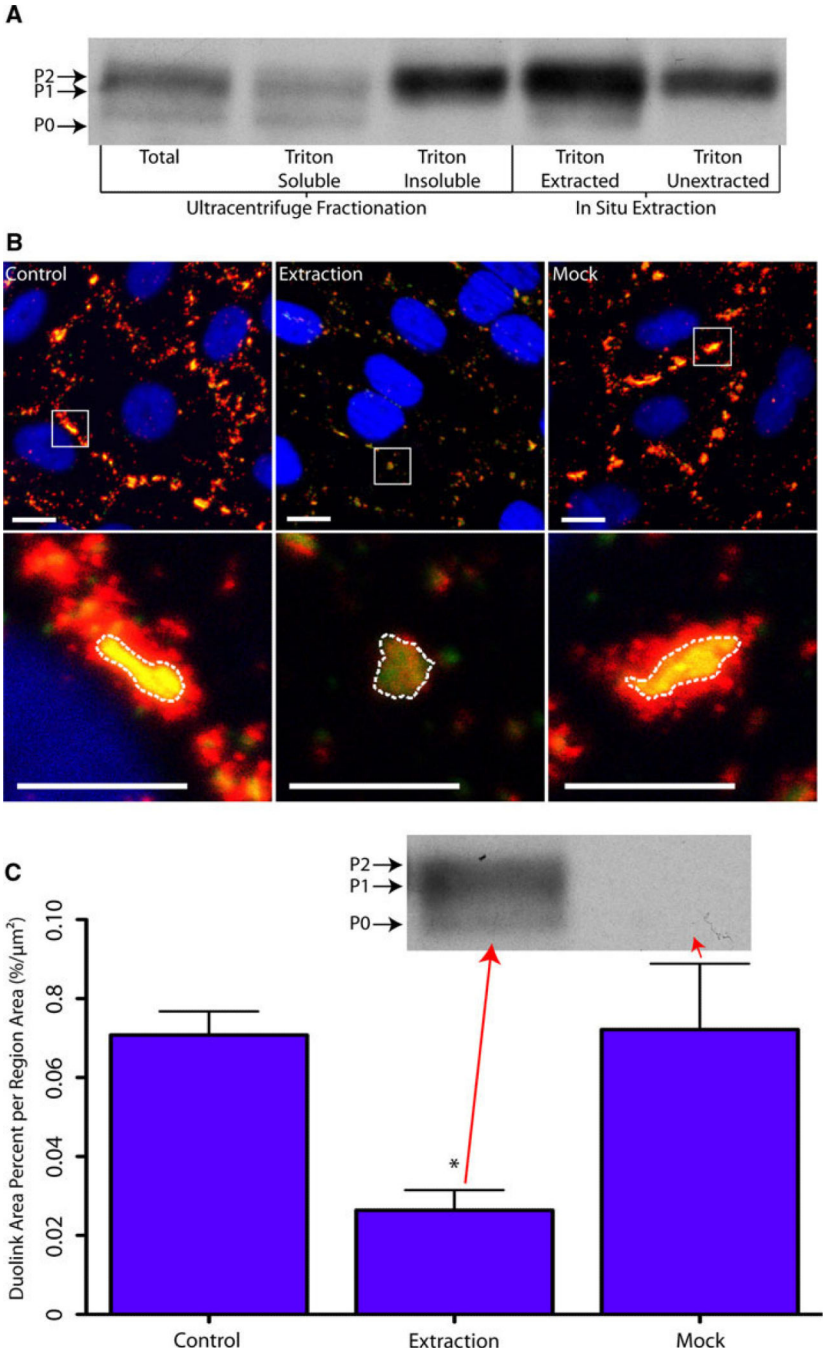

Fig. 3.

Cx43 in the perinexus is nonjunctional. **a** Comparison of Cx43 Western blot banding pattern between cultured NRHM lysates subjected to Triton X-100 fractionation by ultracentrifugation, and cultured NRHMs extracted in situ with Triton X-100. Whole Cx43 lysates (“Total” lane) display the characteristic triple banding pattern corresponding to different phospho-isoforms of Cx43 (P0, P1, and P2). The Triton-soluble and -insoluble fractions of ultracentrifuged lysates display similar banding profiles to Cx43 extracted from NRHM cultures by Triton and the remaining unextracted protein, respectively. **b** Cx43

labeled in NRHM cultures by standard IF (*green*) and high-sensitivity Duolink (*red*). The nucleus is labeled in blue. “Control” cultures were not subjected to in situ Triton extraction; “Extraction” images represent the remaining unextracted protein in cultures treated with buffer containing 1 % Triton X-100 before fixation and staining; “Mock” cultures were treated with the same buffer without Triton before being fixed and stained. **c** Analysis of Duolink staining within the perinexus region (defined as 250–500 nm from the plaque edge) from the experiment in (**b**). Triton extracted cultures displayed a significantly reduced concentration of Cx43 in the perinexus (*$p < 0.05$ vs. “Control”; $n = 4$). The Western blot is labeled for Cx43, probing protein extracted from the cultures labeled in (**b**) in Triton extracted cultures (*left*), and mock extracted cultures (*right*). *Error bars* represent SEM, and *scale bars* represent 10 μm in large images, and 5 μm in expanded images

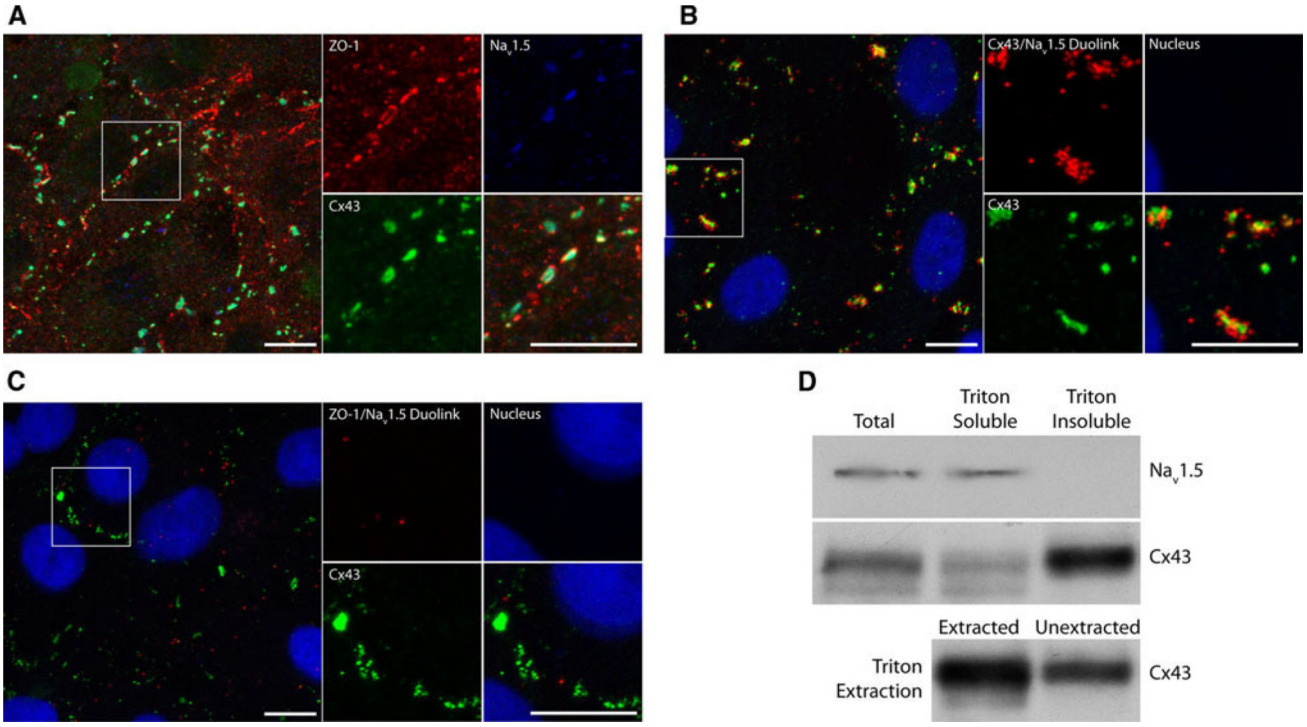

Fig. 4.

Na$_v$1.5 interacts with Cx43, but not ZO-1, in the perinexus of cardiomyocytes. **a** Cultured NRHMs were labeled for Cx43 (*green*), ZO-1 (*red*), and Na$_v$1.5 (*blue*). Note the strong overlap of Cx43 and Na$_v$1.5 signal. **b** Duolink labeling shows Cx43/Na$_v$1.5 interaction at and surrounding GJs in NRHMs. Cx43 is labeled in *green*, Cx43/ Na$_v$1.5 interaction is labeled by Duolink in *red*, and the nucleus is *blue*. **c** Na$_v$1.5 has little or no interaction with ZO-1. Cultured NRHMs were labeled for Cx43 (*green*), ZO-1/Na$_v$1.5 interaction by Duolink (*red*), and the nucleus (*blue*). **d** Triton X-100 fractionated NRHM lysates underwent Western blot analysis for Na$_v$1.5. Clear bands are visible in the whole lysate ("Total" lane) and detergent-soluble fraction ("Triton Soluble" lane), but not the detergent-insoluble fraction ("Triton Insoluble" lane). For comparison, the same Cx43 blots from Fig. 3 are provided, with the Triton fractionation portion being shown in the *middle row*, and the Triton extraction portion being shown in the *bottom row*. *Scale bars* represent 10 μm